ACS APPLIED MATERIALS & INTERFACES

Research Article

www.acsami.org

Facile Synthesis of Conductive Polypyrrole Wrinkle Topographies on Polydimethylsiloxane via a Swelling−Deswelling Process and Their Potential Uses in Tissue Engineering

M. Rifqi Aufan, Yang Sumi, Semin Kim, and Jae Young Lee*

School of Material Science and Engineering, Gwangju Institute of Science and Technology, Gwangju 500-712, Korea

Supporting Information

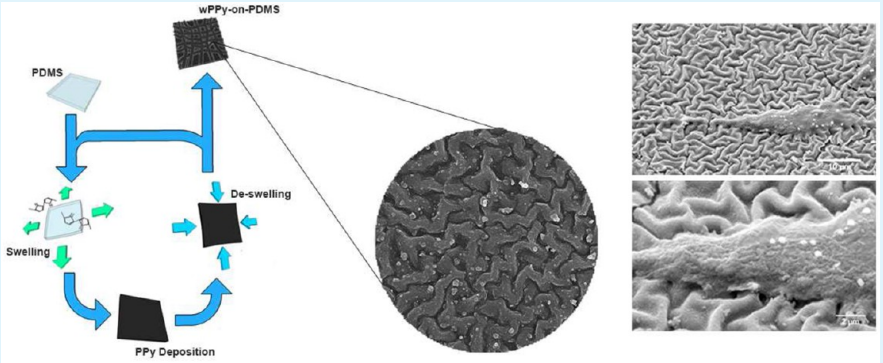

ABSTRACT: Electrically conducting biomaterials have gained great attention in various biomedical studies especially to influence cell and tissue responses. In addition, wrinkling can present a unique topography that can modulate cell−material interactions. In this study, we developed a simple method to create wrinkle topographies of conductive polypyrrole (wPPy) on soft polydimethylsiloxane surfaces via a swelling−deswelling process during and after PPy polymerization and by varying the thickness of the PPy top layers. As a result, various features of wPPy in the range of the nano- and microscales were successfully obtained. In vitro cell culture studies with NIH 3T3 fibroblasts and PC12 neuronal cells indicated that the conductive wrinkle topographies promote cell adhesion and neurite outgrowth of PC12 cells. Our studies help to elucidate the design of the surface coating and patterning of conducting polymers, which will enable us to simultaneously provide topographical and electrical signals to improve cell−surface interactions for potential tissue-engineering applications.

KEYWORDS: *topography, wrinkling, polypyrrole, polydimethylsiloxane, biomaterial*

1. INTRODUCTION

Biomaterials that are electrically conductive and thus can communicate with living systems have garnered considerable attention to actively influence cellular behaviors.[1−3] Electrically conducting polymers (CPs) (e.g., polypyrrole (PPy), polythiophene, poly(3,4-ethylenedioxythiophene) (PEDOT), and polyaniline) have been widely used as attractive biomaterials for various biomedical applications, such as biosensors and tissue-engineering scaffolds, because of their simplicity in synthesis, facile modification of properties, and inherent electroactivity.[4−6] PPy is one of the most studied CPs in the biomedical areas due to its good environmental stability and biocompatibility.[7] In particular, CP-based have been shown to be useful to electrically stimulate various cells, including neurons and cardiomyocytes, and electrically deliver biological molecules to modulate cellular behaviors for potential tissue-engineering applications.[8−13] For example, electrical stimulation via various CP-based scaffolds (e.g., films, nanofibrous meshes, and porous substrates) could promote neurite outgrowth of neuronal cells.[12,11] Furthermore, multifunctional CP biomaterials have been studied to improve cell and CP materials interactions by incorporating various important properties (e.g., bioactivity, porosity, and topography) into CP materials.[14]

Extensive studies have also revealed that topography plays important roles in cell adhesion, proliferation, differentiation, and migration, and has thus been considered an essential parameter in designing biomaterials.[15,16] Various surface patterns, including specific patterns and feature sizes, have been fabricated to mimic the native tissue structures in the human body and, more importantly, to affect cellular behaviors.[17,18] Surface wrinkling is a particularly interesting topography because of its ease of fabrication and unique topological features.[19,20] Wrinkling is a form of mechanical instability that occurs when a thin stiff film of one material bonded to a softer, more compliant substrate experiences a compressive force. Once the compressive force along a certain

Received: June 13, 2015
Accepted: October 7, 2015
Published: October 7, 2015

DOI: 10.1021/acsami.5b09355
ACS Appl. Mater. Interfaces 2015, 7, 23454−23463

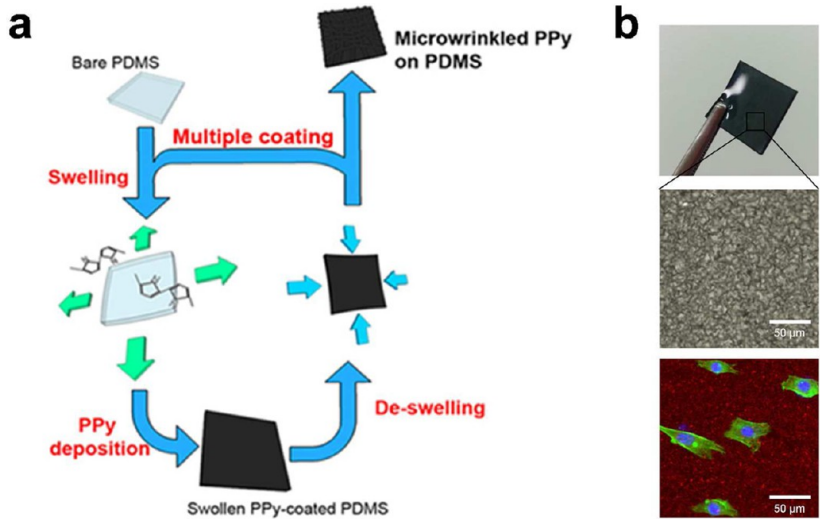

Figure 1. Conductive wrinkle topographies on PDMS. (a) Schematic diagram of wPPy formation by polymerizing PPy on PDMS with different swelling-induced strains and PPy layer thicknesses. (b) Images of PPy wrinkle-coated PDMS for cell culture applications: a photograph of the wPPy-on-PDMS (top), its optical microscopic image (middle), and a fluorescence image of NIH3T3 cells grown on the wPPy substrate (bottom) with staining for F-actin using Alexa 588 labeled phalloidin 24 h after seeding.

direction exceeds a critical value, the thin film buckles and produces wrinkles in the direction perpendicular to the force. On the basis of this principle, Bowden et al. created complex ordered wrinkle structures from thin metal films on polydimethylsiloxane (PDMS) via thermal contraction.[21] They obtained uniform wrinkle wavelength in the range of 20−50 μm and could control the wrinkle orientation by introducing the relief structure on the underlying substrate. Subsequently, various methods have been applied for producing various wrinkle structures such as deposition on a prestretched substrate and induction of thermal shrinkage.[22,23] Wrinkles have been found to benefit several applications, such as flexible electronics, selective adhesion, and thin film metrology, which make surface wrinkling more intriguing to be explored.[24−26] Furthermore, surface wrinkling also has a promising impact on biomaterial areas as it can provide biologically important topographical features that can improve cellular interactions in a simple and controllable manner. For example, Guvendiren and Burdick prepared lamellar and hexagonal wrinkles on photocurable poly(2-hydroxyethyl methacrylate) hydrogels and showed the ability of wrinkle patterns to affect human mesenchymal stem cell morphology and differentiation.[27] Chen et al. demonstrated that wrinkles on polyethylene film could control the orientation of human embryonic stem cells and thus induce their differentiation.[28]

Multifunctional biomaterials that can simultaneously deliver electrical and topographical cues are highly desirable to achieve more intimate cell−material interactions. The surface morphologies of CPs can be varied by simply controlling electrochemical synthetic parameters (e.g., dopant types and concentrations and polymerization time) in general; however, this approach usually leads to relatively random, irregular, and nanometer-scaled small structures.[29,30] Substantial efforts have been made to create specific topographies on CP biomaterials. Gomez et al. electrochemically fabricated PPy micropatterns on lithographic electrode patterns and found that the PPy micropattern features induced faster polarization of embryonic hippocampal neurons compared to flat PPy substrates.[31] Recently, Greco et al. produced anisotropic microwrinkle patterns of PEDOT on thermo-retractable polystyrene by thermal treatment of PEDOT-coated polystyrene at 160 °C.[32] Anisotropic conductive patterns were found to lead to the alignment and differentiation of C2C12 myoblasts. However, this work requires specific conditions, such as thermally shrinking hard materials and annealing at high temperatures, and the parameters that influence wrinkle feature formation were not systemically studied.

Successful nerve tissue regeneration often involves multiple and well-harmonized properties (e.g., extracellular matrix components, growth factors, topographies, and mechanical properties).[33] Therefore, numerous biomaterials have been synthesized and employed for neural tissue applications.[34−36] In particular, Ghasemi-Mobarakeh et al. explained in their review the significant impact of electrical cues for enhancing the nerve regeneration process.[37] Incorporation of CPs with addition of biological molecules can improve cell attachment and proliferation on the scaffold. Dvir et al. explained the benefit of multifunctional scaffolds for compensating several conventional scaffold limitations, such as weak mechanical properties and lack of electrical conductivity.[38] Consequently, multifunctional biomaterials consisting of CPs are particularly desirable for effective modulation of neuronal cells and/or nerve tissue regeneration.

In this study, we aim to fabricate both topographically and electrically active flexible biomaterials in a simple fashion. We create wrinkled PPy patterns (wPPy) on a polydimethylsiloxane (PDMS) surface by deposition of a PPy thin layer under swelling-induced strained conditions. Various conductive wrinkles could be fabricated by varying PDMS swelling-induced strains and the PPy layer thicknesses (Figure 1a). The produced topographical features and electrical properties of the wPPy were characterized. In vitro cell studies with 3T3 fibroblasts and PC12 cells were performed to explore the effects of the conductive wrinkle topographies on cell behavior and the feasibility of potential tissue-engineering applications (Figure 1b).

2. EXPERIMENTAL SECTION

Fabrication of wPPy/PDMS. A thin PDMS film was prepared by mixing a PDMS precursor and a cross-linker (Dow Corning) at a 10:1

DOI: 10.1021/acsami.5b09355
ACS Appl. Mater. Interfaces 2015, 7, 23454−23463

weight ratio. The mixture was then cast onto a polystyrene dish (Nunc) for a thickness of 1 mm and allowed to cure at 60 °C overnight. The cured PDMS was cut into 2 × 2 cm^2 square pieces for the following experiments. For the swelling study, the PDMS piece was transferred into different solvents: double deionized water (DDI), isopropyl alcohol (IPA, Sigma), 1-butanol (BtOH, Sigma), and tetrahydrofuran (THF, Sigma). The PDMS was incubated to make it fully swollen at room temperature for 1 h. The PDMS dimension at the fully swollen state was measured to study a swelling degree. Next, the deswelling was performed by drying the swollen PDMS until no dimensional change was observed. In this process, the PDMS was found to return to its original size with no wrinkle formation on the surfaces after deswelling.

For PPy polymerization and deposition onto the PDMS, pyrrole (Sigma) was first purified by passing it through a column filled with aluminum oxide (Sigma). Purified pyrrole was dissolved at a concentration of 5% (v/v) in individual solvents (DDI, IPA, BtOH, and THF). An oxidant solution was prepared in each solvent with 50 mg/mL $CuCl_2$ (Sigma) and added to each pyrrole-containing solution. The mixtures were allowed to react for 1 h at room temperature and filtered using Whatman filter paper to remove PPy aggregates. The PDMS pieces were incubated in the filtered PPy polymerizing solution for 24 h for PPy deposition. To obtain a thick PPy coating, the coating process was repeated 2 or 3 times. After rinsing with its affiliated solvent, each sample was completely dried at room temperature and sealed for storage. The overall PPy coating process is illustrated in Figure 1a. To prepare smooth PPy-on-PDMS, PPy polymerization and deposition was performed in water, in which PDMS does not swell (no strain during PPy coating). The smooth PPy/PDMS was used as controls for the following cell culture studies.

Wrinkle Morphological Analysis. The morphological structures of the wPPy/PDMSs were analyzed by using a field emission scanning electron microscope (FE-SEM, Hitachi S-4700) and an atomic force microscope (AFM, XE-100 Park System). For SEM analysis, the samples were coated with platinum by sputtering. The wavelength was determined by measuring the distance between consecutive corresponding peaks of the wrinkles observed from SEM images using ImageJ software (NIH) ($n > 20$). The amplitudes of the wPPy were determined using AFM with a noncontact tip (PPP-NCHR, Park System Corp). From the AFM topography images, height profiles were used to analyze the amplitude of wrinkles, which was defined to the distance between the peak and the valley of the wrinkle ($n > 20$). Averages ± standard deviations are presented.

Surface Resistance Measurement. For sheet resistance (R_s) measurements, the wPPy sample was contacted with two copper electrodes connected to a multimeter (Extech 430). From the resistance (R), the sheet resistance was calculated using an equation of $R_s = R \times (W/D)$, in which D and W indicate the distance between the two electrodes and the width of each electrode, respectively. The average sheet resistance value was obtained from multiple measurements ($n = 5$). The conductivity was then calculated using the relationship: conductivity (σ) = 1/(film thickness × R_s). Averages ± standard deviations are presented.

Water Contact Angle Measurement. Contact angle goniometer (Pheonix 300, SEO Co. Ltd.) was used to measure the water contact angles of various wPPy substrates by the Sessile drop method. A pure water drop (5 μL) was placed on the surface of the substrate in the air at room temperature. $n = 3$. Averages ± standard deviations are reported.

In Vitro Cell Culture. Mouse NIH 3T3 fibroblasts were maintained in Dulbecco's modified eagle's medium (DMEM, Invitrogen) supplemented with 10% fetal bovine serum (Invitrogen) and 1% penicillin-streptomycin (Invitrogen) at 37 °C in a 5% CO_2 incubator. The medium was changed every other day. For experiments with the wPPy samples, cells were seeded at a density of 5 × 10^3 cell/cm^2 on each substrate. PC12 cells were maintained in DMEM supplemented with 10% heat-inactivated horse serum (Invitrogen), 5% fetal bovine serum, 1% penicillin-streptomycin, and 1% nonessential amino acid solution (100×, Invitrogen) at 37 °C in a humidified incubator with a 5% CO_2 atmosphere. For experiments with the wPPy samples, PC12 cells were primed by treating with 100 ng/mL nerve growth factor (7S NGF, Promega) 3 days before cell seeding. The substrate was treated with collagen (1 μg/mL, 5 min) (Invitrogen). PC12 cells were seeded onto each substrate at a density of 5 × 10^3 cell/cm^2 and incubated in the NGF-containing culture medium for 1, 3, and 5 days.

Immunostaining and Image Analysis. After incubation, the samples were fixed by 3.7% para-formaldehyde solution for 15 min. To stain F-actin, the samples were incubated in 0.1% Triton X-100 (in PBS) (Sigma) for 5 min, followed by incubation in a blocking solution (1% bovine serum albumin (BSA, Sigma) in PBS) for 15 min. Then the samples were incubated in Alexa-488-conjugated phalloidin (1:500, Invitrogen) in the blocking solution at room temperature for 30 min. After being washed with PBS, the samples were further incubated with 4′,6-diamidino-2-phenylindole (DAPI, 1 μg/mL, Invitrogen) for 5 min. The samples were then washed three times using PBS. The fluorescence images were taken using a microscope (Leica DMI3000B). From the acquired images, adherent cell numbers on the sample were counted from the randomly selected images ($n > 5$). The average and standard deviation were reported. For the cell morphological analysis, cell circularity was calculated from the acquired fluorescence images. ImageJ software (NIH) was used for measuring the circularity of the cells with the formula, $(4\pi A)/P^2$, in which the measured perimeter (P) of an individual cell was divided by the circumference of a circle with the same area (A). Thus, a circularity of 1 indicates an ideal circle. More than 100 cells were analyzed and the statistical significance was assessed using a Student t-test with Origin software. The neuritogenesis of PC12 cells was analyzed from fluorescence images using ImageJ software. An individual neurite length was measured as a linear distance from the soma to the end of neurite. A neurite was defined and considered when it was longer than 15 μm. The percentage of neurite-bearing cells and the lengths of individual neurites were measured and reported for each sample. More than 130 cells were analyzed and the statistical significance was assessed using a Student t-test with Origin software.

SEM Imaging of Cells on wPPy. For the investigation of interactions between cells and wPPy, PC12 cells were cultured on wPPy[IPA1] for 5 days as mentioned above. Then the substrates were fixed with 5% gluteraldehyde solution (in PBS), rinsed with DDI water, and dried in the air overnight. The substrates were coated with platinum using a sputter coater. SEM images were obtained by using a field emission scanning electron microscope (JEOL JSM-7500F).

3. RESULTS AND DISCUSSION

Wrinkle structures are in general influenced by material properties (i.e., Young's modulus and Poisson's ratio), strain, and layer thickness.[39] In our system, swelling-induced straining of a PDMS film in organic solvents and PPy deposition on the PDMS was employed to form conductive PPy wrinkle features. The swelling-induced straining and deswelling processes were expected to cause compressive force necessary to trigger wrinkle formation. Additionally, the PPy layer thickness was considered as another parameter that could affect the feature dimensions of the resultant PPy wrinkles. First, the swelling of PDMS in various solvents was examined to study different straining conditions resulting in various swelling degrees of PDMS.[40] We tested isopropyl alcohol (IPA), 1-butanol (BuOH), and tetrahydrofuran (THF) and found PDMS swelling in the following order: THF > BuOH > IPA. THF caused the highest PDMS swelling with a 40 ± 3.7% increase in length, while the incubation of PDMS in BuOH and IPA solvents led to 20 ± 1.9% and 5 ± 0.2% length increases, respectively. Different degrees of swelling-induced strain in these organic solvents could be applied for synthesis of the following PPy wrinkles (wPPy). For PPy deposition, the fully swollen PDMS substrate was subsequently transferred into a PPy polymerization solution consisting of pyrrole monomer,

DOI: 10.1021/acsami.5b09355
ACS Appl. Mater. Interfaces 2015, 7, 23454−23463

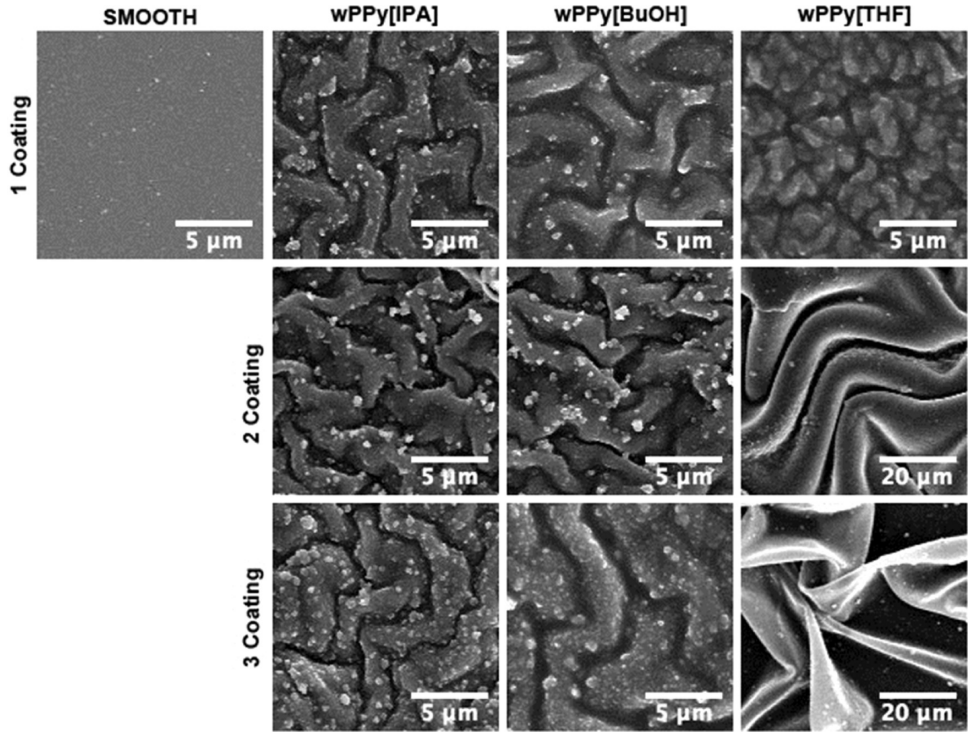

Figure 2. Scanning electron micrographs of various wPPy substrates. (a) Top views of wPPy synthesized using different solvents and PPy coating numbers. Smooth PPy/PDMS was produced using water.

Table 1. wPPy Samples and Their Topographical Features[a]

samples	solvent	coating no.	thickness (μm)	wavelength (μm)	amplitude (μm)
wPPy[IPA1]	IPA	1	0.18 ± 0.01	2.94 ± 0.33	0.36 ± 0.03
wPPy[IPA2]		2	0.23 ± 0.02	3.58 ± 0.64	0.64 ± 0.04
wPPy[IPA3]		3	0.25 ± 0.02	4.36 ± 0.63	1.20 ± 0.04
wPPy[BuOH1]	BuOH	1	0.17 ± 0.01	2.86 ± 0.39	0.52 ± 0.03
wPPy[BuOH2]		2	0.23 ± 0.02	3.72 ± 0.61	0.72 ± 0.05
wPPy[BuOH3]		3	0.24 ± 0.02	4.71 ± 0.78	1.32 ± 0.04
wPPy[THF1]	THF	1	0.13 ± 0.02	1.55 ± 0.27	0.42 ± 0.02
wPPy[THF2]		2	0.17 ± 0.02	N/A[b]	N/A[b]
wPPy[THF3]		3	0.22 ± 0.02	N/A[b]	N/A[b]

[a]Averages ± standard deviations are represented. [b]N/A: not applicable due to frequent delamination.

oxidant ($CuCl_2$), and the same solvent as used in the swelling of the PDMS substrate. Incubation in the PPy polymerization solution permits the deposition of PPy onto solid substrates (e.g., PDMS film) as reported in the literature.[41] PPy polymerization under optimized conditions could provide the uniform PPy coating with well-defined structures.[41,42] The substrate turned black after PPy polymerization, indicating successful chlorine-doped PPy deposition on the PDMS (Figure 1S of the Supporting Information). To increase the PPy layer thickness, we repeated the PPy coating procedures using the same solvents for two and three repetitions. The wPPy prepared on PDMS under various conditions was denoted as wPPy[solvent_coating number]. For example, wPPy[IPA2] indicates the substrate that was prepared with two PPy coatings on PDMS using IPA solvent. Because water does not cause PDMS to swell, the polymerization and deposition of PPy on PDMS in water resulted in a smooth surface without substantial PPy wrinkling, which was used as smooth controls for the cell culture studies later.

A morphological investigation of PPy wrinkles (wPPy) was performed using a scanning electron microscope (SEM) and an atomic force microscope (AFM) (Figure 2S). As shown in Figure 2, wPPy with a variety of features on the PDMS produced under different conditions was obtained. The analytical results indicate that the wPPy had features of a few micrometer-sized wavelengths and hundreds of nanometer-sized amplitudes (Table 1). The wPPy features were influenced by the type of solvent used (i.e., strain) and the PPy top layer thickness. Higher strains caused the lower wavelength of the wPPy patterns. As shown in Table 1, wPPy[THF1] had the lowest wrinkle wavelength (1.55 ± 0.27 μm) followed by wPPy[BuOH1] (2.86 ± 0.39 μm) and wPPy[IPA1] (2.94 ± 0.33 μm), which is approximately inversely related to the swelling degrees of PDMS. In addition, with an increase in the PPy layer thickness (multiple coating steps), larger wrinkles were formed. For example, after three coatings, wPPy[IPA3] and wPPy[BuOH] had large features with >4 μm wavelength and >1 μm amplitude. PPy layer thicknesses after a single coating were in the range of 130−180, while multiple coatings

DOI: 10.1021/acsami.5b09355
ACS Appl. Mater. Interfaces 2015, 7, 23454−23463

increased the thickness up to ~250 nm. Interestingly, the thicknesses of the PPy layers were found different depending on the solvent type. PPy polymerization solvents can influence PPy polymerization rates, deposition, and substrate surface area exposed for PPy deposition,[43,44] which appear to result in different thickness of the wPPy layers in different solvents. This thickness, together with the strain due to the swelling, affects the overall wPPy formation and its structures, suggesting the possibility of control over the topography and further design of wPPy by employing different synthesis conditions. However, the resultant wPPy features often appeared not very regular and stable especially for the wPPy synthesized under high straining with a thick layer (e.g., wPPy[THF2] and wPPy[THF3]). This may be due to heterogeneous traction forces during a deswelling process, nonuniform PPy coating, and local buckling. The wPPy films produced with low straining and small layer thickness were well attached onto the PDMS (Figure 3S), likely due to good molecular interactions such as hydrophobic interactions.[45−47] On the other hand, in certain cases where the samples were produced in a high swelling solvent and with a thick PPy layer, wPPy[THF2] and wPPy[THF3], the wPPy layers were often found to be seriously delaminated, showing inhomogeneous features. Delamination buckling takes place when the traction force being caused during deswelling at the interface between PDMS and PPy exceeds their bonding force. Thus, it will be important to adjust straining and PPy deposition thickness and improve PDMS−PPy layer adhesion not to exceed its critical delamination point, which still remains a challenge when employing highly swelling solvents in this system.

The electrical properties of wPPy were measured (Figure 3). wPPy[THF1] had a sheet resistance (R_s) of ~1 MΩ/sq, and

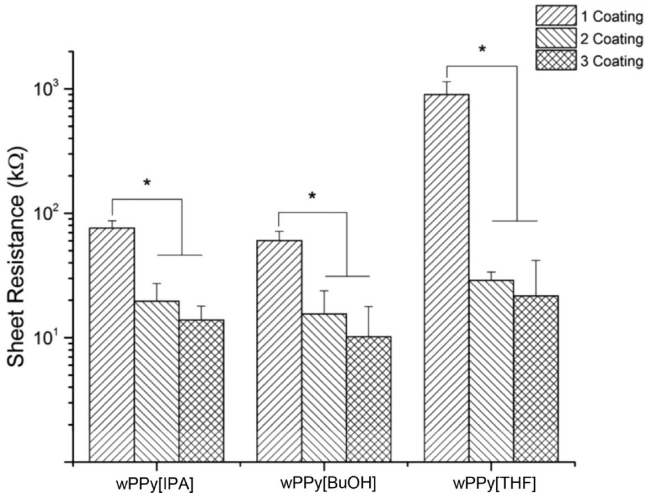

Figure 3. Sheet resistances of various wPPy substrates synthesized using different solvents and coating numbers. Averages ± standard deviations are plotted. (* denotes $p < 0.05$).

the wPPy[IPA1] and wPPy[BuOH1] samples showed R_s values in the range of 70−100 kΩ/sq. R_s was found to decrease with an increase in deposition steps (i.e., the increased thickness of the wPPy layer), as expected. After three coatings, the R_s value was 12, 14, and 57 kΩ/sq for wPPy[IPA3], wPPy[BuOH3], and wPPy[THF3], respectively. The results indicate that sheet resistance of the substrates is mainly inversely related to the conducting layer thickness. Electrical conductivity of the wPPy layers of the wPPy[IPA] and wPPy[BuOH] was in the range of 1−10 S/cm, whereas conductivity of wPPy[THF] was 0.1−1 S/cm. Overall, wPPy[THF] samples showed higher resistances compared to wPPy[IPA] and wPPy[BuOH]. We speculate that it might result from mechanical instability of wPPy caused by high strains in THF, longer effective lengths of conductive layers on wPPy[THF], and the possible negative effects of THF solvent on electrical properties of the PPy. Nevertheless, the electrical activity of wPPy will be appropriate to the simultaneous delivery of topographical and electrical cues for potential uses in tissue engineering.[48]

Prior to the cell experiments, we examine the wettability and protein adsorption with wPPy[IPA] samples and smooth controls. Wettability is influenced by surface properties.[49,50] wPPy[IPA1] and wPPy[IPA2] had higher water contact angles (114 ± 7° and 120 ± 5°, respectively) compared to the smooth controls (96 ± 1°). These high water contact angles appear to result from the rough surface structures that can possess air in the structures.[51] Water contact angle of wPPy[IPA3] was decreased to 97 ± 1°, likely due to larger wrinkles that may not trap air on the surfaces. In addition, protein adsorption studies with BSA indicated that wPPy[IPA] showed more protein adsorption compared to the smooth controls, which may be due to larger effective surface areas of the PPy layers compared to the smooth substrates (Figure S5).

To examine the effects of wPPy on cellular behavior, NIH-3T3 cells were cultured on the wPPy[IPA] series as representing conductive topographic substrates. Smooth PPy substrates were also prepared in water solution as control substrates. Figure 4a−d shows representative images of NIH 3T3 fibroblasts cultured on smooth PPy and wPPy[IPA]. As shown in Figure 4e, more cells adhered on wPPy[IPA1] than on the smooth controls, wPPy[IPA2], and wPPy[IPA3], suggesting that the topographies presented by wPPy[IPA1] provide better features for cell adhesion. A number of studies have demonstrated that specific surface features lead to specific cellular responses including cell attachment.[16,18] The introduction of specific subcellular scaled surface features often promote cell adhesion. For example, Park et al. generated various vertically oriented TiO_2 nanotubes with 10−100 nm diameters for human mesenchymal stem cell (hMSC) culture.[52] They determined that the surfaces of 15 nm TiO_2 nanotubes were optimal for the adhesion and differentiation of hMSCs. Murphy and colleagues found that SV 40 human corneal epithelial cells adhered more and strongly on silicon substrates with groove features of 400 nm pitch dimension compared to those with smooth and larger patterns.[53] Promotion of cell adhesion onto biomaterials, including conducting materials, will be generally beneficial because cell adhesion is pivotal to achieve intimate cell−biomaterial interactions and tissue development.[54] Moreover, in our study, the cells on the wPPy also displayed more elongated shapes on the wPPy compared to the cells on the smooth PPy controls (Figure 4f). These morphological differences were analyzed in terms of the circularity parameter.[55] The circularity values of the cells on the wPPy samples were significantly lower (0.4−0.5) than those of the cells on the smooth controls (~0.69). Thakar et al. observed a similar result, in which fibroblasts and skeletal myoblasts on PDMS substrates with microscale protrusions were significantly elongated compared to those observed on nonpatterned PDMS controls.[56] Wrinkle topographies can affect the cellular interactions with substrates, which eventually cause changes in the cytoskeleton structure and distribution. The morpho-

DOI: 10.1021/acsami.5b09355
ACS Appl. Mater. Interfaces 2015, 7, 23454−23463

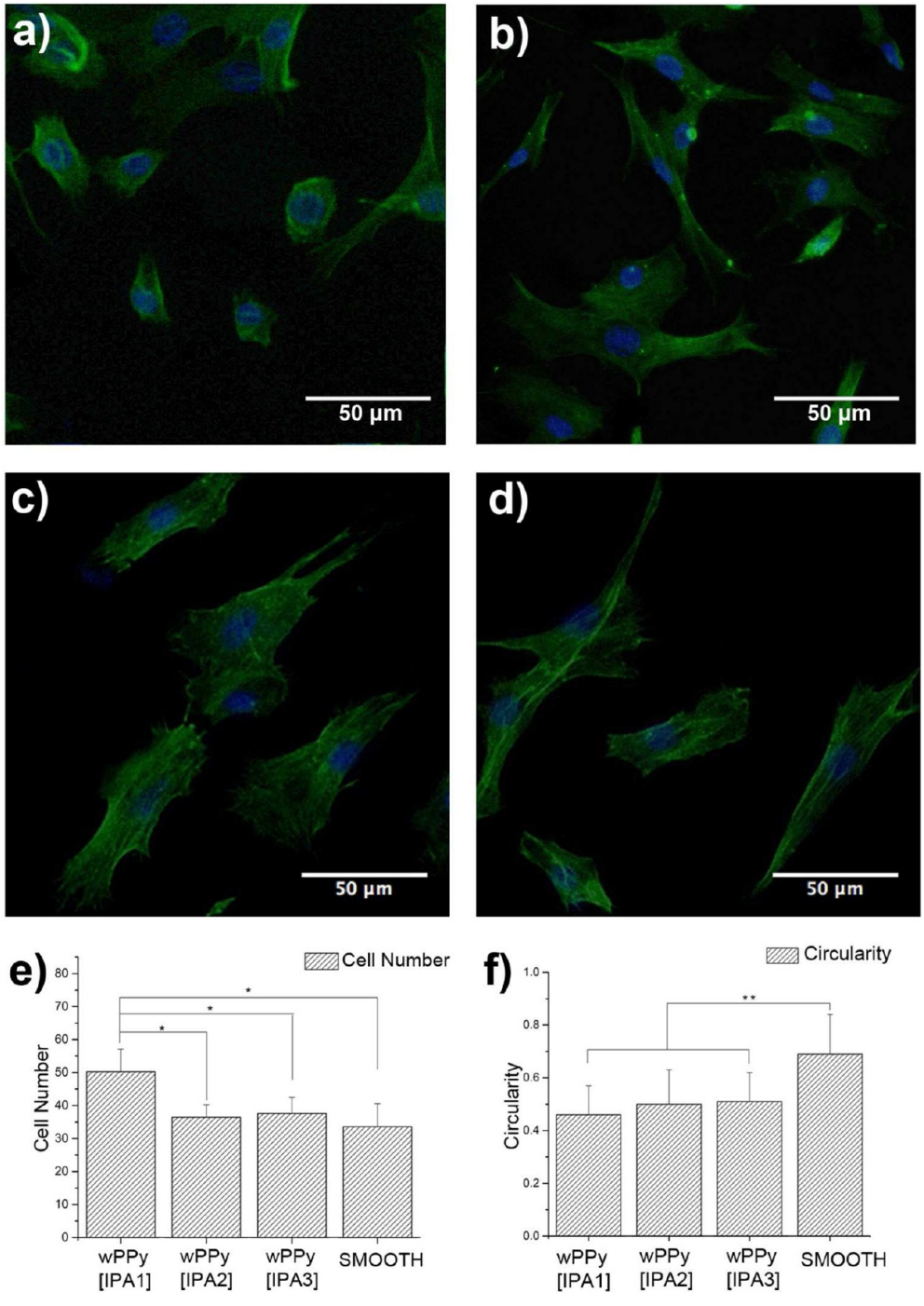

Figure 4. Immunostaining images of 3T3 cells on (a) smooth, (b) wPPy[IPA1], (c) wPPy[IPA2], and (d) wPPy[IPA3]. After 48 h in culture, cells were fixed and stained for nuclei (blue) and F-actin (green). Analytical results of (e) the adherent cell numbers and (f) the circularity values. Averages ± standard deviations are plotted. (* denotes $p < 0.05$, ** denotes $p < 0.01$).

logical difference among the cells implies that the fibroblasts can sense and interact with the subcellular-sized wrinkles and exhibit different cytoskeletal organization from the cells on the smooth substrates.

PC12 neuronal cells were tested to study the effects of the wPPy features on neurite outgrowth for potential neural tissue applications. For PC12 cells, we used the wPPy[IPA1] and smooth PPy controls for comparison. Both wPPy and smooth PPy supported good PC12 cell growth (Figure 5). On day 1, more adherent cells were found on the wPPy[IPA1] than on the smooth PPy. This observation is similar to the case of the 3T3 fibroblasts on the wPPy, implying that topography of the wPPy[IPA1] can be supportive of the initial attachment of multiple cell types to substrates. Cell numbers increased during incubation. Interestingly, more cells were observed on the smooth PPy than on the wPPy[IPA1] on day 3. It may be possible that the smooth surface may induce proliferation of PC12 cells, whereas the wPPy[IPA1] helps the initial attachment of the cells.

The PC12 cells on the wPPy-promoted neurite formation, resulting in more neurite-bearing cells (73.7 ± 13.1%) than on its smooth counterpart (56.8 ± 11.7%) after 5 days of

DOI: 10.1021/acsami.5b09355
ACS Appl. Mater. Interfaces 2015, 7, 23454−23463

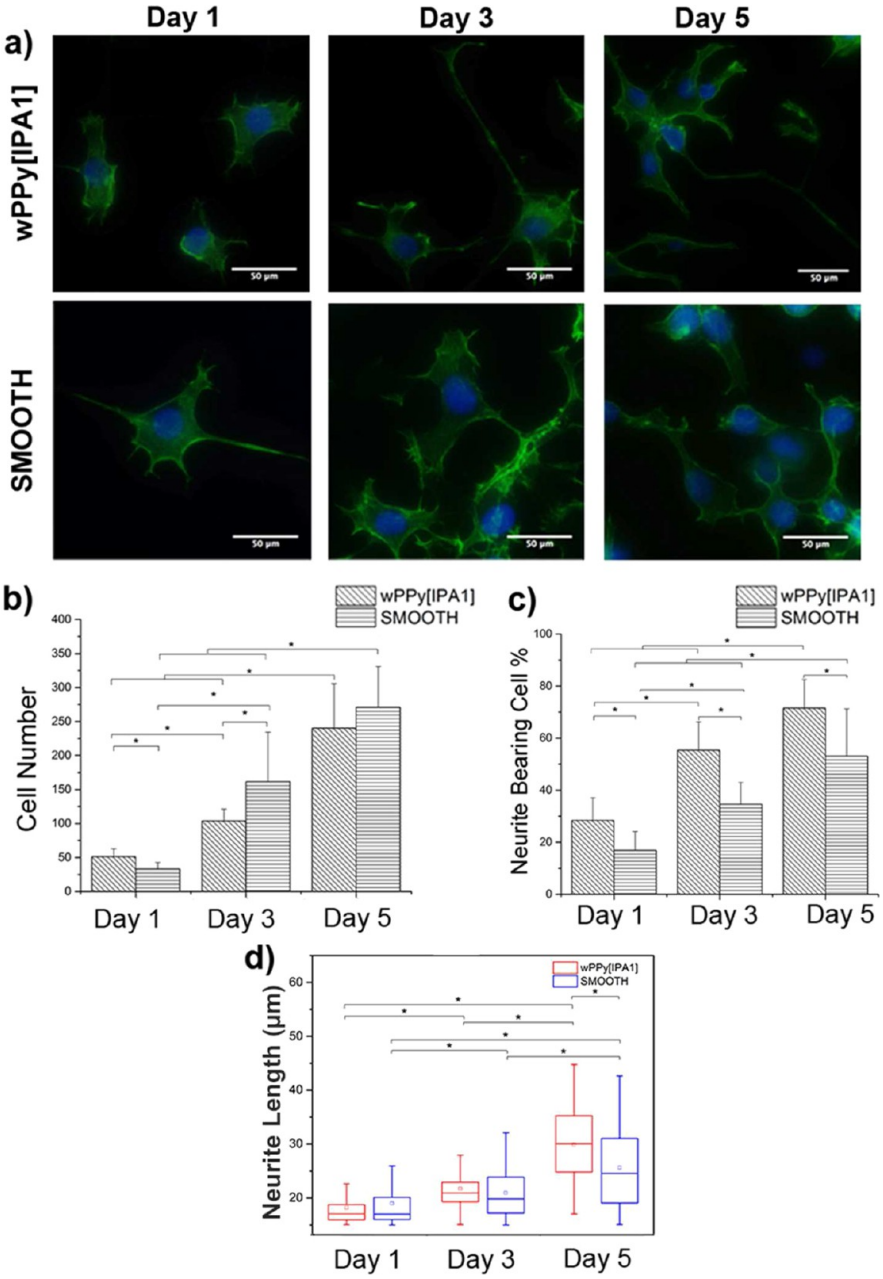

Figure 5. Effects of conductive wrinkle substrates on PC12 neuronal cells. (a) Immunostaining images of PC12 neuronal cells cultured on wPPy[IPA1] and smooth PPy for 1, 3, and 5 days. Cells were fixed and stained for nuclei (blue) and F-actin (green). Analytical results of (b) cell numbers, (c) percentages of the neurite bearing cells, and (d) neurite length of PC12 cells cultured on smooth and wPPy[IPA1]. Averages ± standard deviations are plotted (* denotes $p < 0.05$).

incubation (Figure 5c). Similar results regarding induced neurite outgrowth on subcellular-scaled topographies were previously reported.[57] Su et al. studied the effects of micropatterns on PC12 cell behaviors and found that the cells cultured on Si microgrooved patterns extended 2 to 3 times longer neurites on the micropatterns.[58] Foley et al. observed that PC12 cells formed neurites at lower NGF concentrations on topographic patterns, whereas cells on smooth substrates required high NGF concentrations to have similar neurite formation.[59] On the wPPy[IPA1], smaller cell numbers and more neurite-forming cells were found compared to those on the smooth PPy. When considering both cell numbers and neurite forming cells together, it appears that the cells on the wPPy[IPA1] prefer differentiation (i.e., neurite formation) to proliferation, whereas the cells on the smooth substrate tend to induce proliferation rather than neurite formation. Regarding neurite elongation, in our study, no significant differences in neurite length were found between the wPPy and smooth PPy substrates during the early days of culture. However, significantly longer neurites were found on the wrinkled topographies at day 5 (Figure 5d). However, at day 5, the neurite lengths on the wrinkled topographies were between 15 and 45 μm, with 50% having lengths greater than 25 μm. On the other hand, PC12 cells cultured on the smooth samples had only 25% of neurites longer than 27 μm. The SEM images of PC12 cells on wPPy[IPA1] show that cells grow well on the micrometer-scale PPy wrinkles over the surface and neurites and filopodia intimately interact with wrinkle

DOI: 10.1021/acsami.5b09355
ACS Appl. Mater. Interfaces 2015, 7, 23454−23463

structures (Figure 6). Topographies have been suggested to affect growth cone behaviors and focal contact formation of

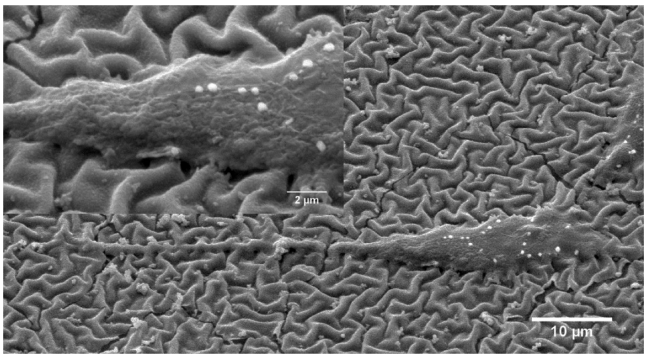

Figure 6. Scanning electron micrographs of PC12 cells on wPPy[IPA1].

neuronal cells, potentially resulting in promoted neurite outgrowth. As a result, our conductive wrinkle patterns will be very useful to induce neuronal adhesion and differentiation for neural tissue regeneration applications.

4. CONCLUSION

Both electrically and topographically active biomaterials are highly desired for studies to understand and improve cell−material interactions. In this study, we demonstrated the simple formation of various conductive PPy wrinkles on PDMS by controlling the strain during PPy deposition and the PPy layer thickness. In vitro cell culture studies with micrometer-sized conductive wrinkle features using 3T3 fibroblasts and PC12 neuronal cells indicated that wPPy substrates could influence cellular behaviors, such as increased cell adhesion, changes in morphology, and promotion of neurite outgrowth. Future studies will include fine control over wPPy wrinkle features and the electrical stimulation of cells grown on wrinkled PPy and precise studies on the combinatorial roles of topographical and electrical cues on cells. Our wPPy-on-PDMS materials offer a novel design strategy for biomaterials for potential tissue-engineering scaffold applications.

■ ASSOCIATED CONTENT

Supporting Information

Schematic images of wPPy-formed PDMS and its cell culture application, photographs of bare PDMS and wPPy−PDMS, and representative AFM images of various wPPy substrates and their height profiles. The Supporting Information is available free of charge on the ACS Publications website at DOI: 10.1021/acsami.5b09355.

■ AUTHOR INFORMATION

Corresponding Author

*E-mail: jaeyounglee@gist.ac.kr.

Author Contributions

The manuscript was written through contributions of all authors. All authors have given approval to the final version of the manuscript.

Notes

The authors declare no competing financial interest.

■ ACKNOWLEDGMENTS

This research was supported by the Global Research Lab Program (2013-050616), the Pioneer Research Center Program (NRF-2014M3C1A3001208), and Basic Science Research Program (2013R1A1A1012179) through the National Research Foundation of Korea (NRF) funded by the Ministry of Science, ICT & Future Planning. This research was also supported by a grant of the Korea Health Technology R&D Project through the Korea Health Industry Development Institute (KHIDI), funded by the Ministry of Health & Welfare, Republic of Korea (H I14C3484).

■ REFERENCES

(1) Hardy, J. G.; Lee, J. Y.; Schmidt, C. E. Biomimetic Conducting Polymer-Based Tissue Scaffolds. *Curr. Opin. Biotechnol.* **2013**, *24*, 847−854.
(2) Wallace, G. G.; Higgins, M. J.; Moulton, S. E.; Wang, C. Nanobionics: The Impact of Nanotechnology on Implantable Medical Bionic Devices. *Nanoscale* **2012**, *4*, 4327−4347.
(3) Guimard, N. K.; Gomez, N.; Schmidt, C. E. Conducting Polymers in Biomedical Engineering. *Prog. Polym. Sci.* **2007**, *32*, 876−921.
(4) Balint, R.; Cassidy, N. J.; Cartmell, S. H. Conductive Polymers: Towards a Smart Biomaterial for Tissue Engineering. *Acta Biomater.* **2014**, *10*, 2341−2353.
(5) Herlogsson, L.; Crispin, X.; Robinson, N. D.; Sandberg, M.; Hagel, O.-J.; Gustafsson, G.; Berggren, M. Low-Voltage Polymer Field-Effect Transistors Gated via a Proton Conductor. *Adv. Mater.* **2007**, *19*, 97−101.
(6) Leleux, P.; Badier, J.-M.; Rivnay, J.; Bénar, C.; Hervé, T.; Chauvel, P.; Malliaras, G. G. Conducting Polymer Electrodes for Electro-encephalography. *Adv. Healthcare Mater.* **2014**, *3*, 490−493.
(7) Schmidt, C. E.; Shastri, V. R.; Vacanti, J. P.; Langer, R. Stimulation of Neurite Outgrowth Using an Electrically Conducting Polymer. *Proc. Natl. Acad. Sci. U. S. A.* **1997**, *94*, 8948−8953.
(8) Nishizawa, M.; Nozaki, H.; Kaji, H.; Kitazume, T.; Kobayashi, N.; Ishibashi, T.; Abe, T. Electrodeposition of Anchored Polypyrrole Film on Microelectrodes and Stimulation of Cultured Cardiac Myocytes. *Biomaterials* **2007**, *28*, 1480−1485.
(9) Richardson, R. T.; Thompson, B.; Moulton, S.; Newbold, C.; Lum, M. G.; Cameron, A.; Wallace, G.; Kapsa, R.; Clark, G.; O'Leary, S. The Effect of Polypyrrole with Incorporated Neurotrophin-3 on the Promotion of Neurite Outgrowth from Auditory Neurons. *Biomaterials* **2007**, *28*, 513−523.
(10) Thompson, B. C.; Moulton, S. E.; Richardson, R. T.; Wallace, G. G. Effect of the Dopant Anion in Polypyrrole on Nerve Growth and Release of a Neurotrophic Protein. *Biomaterials* **2011**, *32*, 3822−3831.
(11) Hsiao, C.-W.; Bai, M.-Y.; Chang, Y.; Chung, M.-F.; Lee, T.-Y.; Wu, C.-T.; Maiti, B.; Liao, Z.-X.; Li, R.-K.; Sung, H.-W. Electrical Coupling of Isolated Cardiomyocyte Clusters Grown on Aligned Conductive Nanofibrous Meshes for Their Synchronized Beating. *Biomaterials* **2013**, *34*, 1063−1072.
(12) Shi, Z.; Gao, H.; Feng, J.; Ding, B.; Cao, X.; Kuga, S.; Wang, Y.; Zhang, L.; Cai, J. In Situ Synthesis of Robust Conductive Cellulose/Polypyrrole Composite Aerogels and Their Potential Application in Nerve Regeneration. *Angew. Chem., Int. Ed.* **2014**, *53*, 5380−5384.
(13) Lee, J. Y.; Bashur, C. A.; Goldstein, A. S.; Schmidt, C. E. Polypyrrole-Coated Electrospun PLGA Nanofibers for Neural Tissue Applications. *Biomaterials* **2009**, *30*, 4325−4335.
(14) Li, G. N.; Hoffman-Kim, D. Tissue-Engineered Platforms of Axon Guidance. *Tissue Eng., Part B* **2008**, *14*, 33−51.
(15) Nikkhah, M.; Edalat, F.; Manoucheri, S.; Khademhosseini, A. Engineering Microscale Topographies to Control the Cell−substrate Interface. *Biomaterials* **2012**, *33*, 5230−5246.
(16) Hoffman-Kim, D.; Mitchel, J. A.; Bellamkonda, R. V. Topography, Cell Response, and Nerve Regeneration. *Annu. Rev. Biomed. Eng.* **2010**, *12*, 203−231.

DOI: 10.1021/acsami.5b09355
ACS Appl. Mater. Interfaces 2015, 7, 23454−23463

(17) Qi, L.; Li, N.; Huang, R.; Song, Q.; Wang, L.; Zhang, Q.; Su, R.; Kong, T.; Tang, M.; Cheng, G. The Effects of Topographical Patterns and Sizes on Neural Stem Cell Behavior. *PLoS One* **2013**, *8*, e59022.
(18) Ross, A. M.; Jiang, Z.; Bastmeyer, M.; Lahann, J. Physical Aspects of Cell Culture Substrates: Topography, Roughness, and Elasticity. *Small* **2012**, *8*, 336−355.
(19) Hendricks, T. R.; Wang, W.; Lee, I. Buckling in Nanomechanical Films. *Soft Matter* **2010**, *6*, 3701−3706.
(20) Chen, C.-M.; Yang, S. Wrinkling Instabilities in Polymer Films and Their Applications. *Polym. Int.* **2012**, *61*, 1041−1047.
(21) Bowden, N.; Brittain, S.; Evans, A. G.; Hutchinson, J. W.; Whitesides, G. M. Spontaneous Formation of Ordered Structures in Thin Films of Metals Supported on an Elastomeric Polymer. *Nature* **1998**, *393*, 146−149.
(22) Lacour, S. P.; Wagner, S.; Huang, Z.; Suo, Z. Stretchable Gold Conductors on Elastomeric Substrates. *Appl. Phys. Lett.* **2003**, *82*, 2404−2406.
(23) Chan, E. P.; Crosby, A. J. Fabricating Microlens Arrays by Surface Wrinkling. *Adv. Mater.* **2006**, *18*, 3238−3242.
(24) Khang, D.-Y.; Jiang, H.; Huang, Y.; Rogers, J. A. A Stretchable Form of Single-Crystal Silicon for High-Performance Electronics on Rubber Substrates. *Science* **2006**, *311*, 208−212.
(25) Vajpayee, S.; Khare, K.; Yang, S.; Hui, C.-Y.; Jagota, A. Adhesion Selectivity Using Rippled Surfaces. *Adv. Funct. Mater.* **2011**, *21*, 547−555.
(26) Chung, J. Y.; Lee, J.-H.; Beers, K. L.; Stafford, C. M. Stiffness, Strength, and Ductility of Nanoscale Thin Films and Membranes: A Combined Wrinkling−Cracking Methodology. *Nano Lett.* **2011**, *11*, 3361−3365.
(27) Guvendiren, M.; Burdick, J. A. The Control of Stem Cell Morphology and Differentiation by Hydrogel Surface Wrinkles. *Biomaterials* **2010**, *31*, 6511−6518.
(28) Chen, A.; Lieu, D. K.; Freschauf, L.; Lew, V.; Sharma, H.; Wang, J.; Nguyen, D.; Karakikes, I.; Hajjar, R. J.; Gopinathan, A.; et al. Shrink-Film Configurable Multiscale Wrinkles for Functional Alignment of Human Embryonic Stem Cells and Their Cardiac Derivative. *Adv. Mater.* **2011**, *23*, 5785−5791.
(29) Silk, T.; Hong, Q.; Tamm, J.; Compton, R. G. AFM Studies of Polypyrrole Film Surface Morphology I. The Influence of Film Thickness and Dopant Nature. *Synth. Met.* **1998**, *93*, 59−64.
(30) Gelmi, A.; Higgins, M. J.; Wallace, G. G. Physical Surface and Electromechanical Properties of Doped Polypyrrole Biomaterials. *Biomaterials* **2010**, *31*, 1974−1983.
(31) Gomez, N.; Lee, J. Y.; Nickels, J. D.; Schmidt, C. E. Micropatterned Polypyrrole: A Combination of Electrical and Topographical Characteristics for the Stimulation of Cells. *Adv. Funct. Mater.* **2007**, *17*, 1645−1653.
(32) Greco, F.; Fujie, T.; Ricotti, L.; Taccola, S.; Mazzolai, B.; Mattoli, V. Microwrinkled Conducting Polymer Interface for Anisotropic Multicellular Alignment. *ACS Appl. Mater. Interfaces* **2013**, *5*, 573−584.
(33) Tam, R. Y.; Fuehrmann, T.; Mitrousis, N.; Shoichet, M. S. Regenerative Therapies for Central Nervous System Diseases: A Biomaterials Approach. *Neuropsychopharmacology* **2014**, *39*, 169−188.
(34) Nagamine, K.; Hirata, T.; Okamoto, K.; Abe, Y.; Kaji, H.; Nishizawa, M. Portable Micropatterns of Neuronal Cells Supported by Thin Hydrogel Films. *ACS Biomater. Sci. Eng.* **2015**, *1*, 329−334.
(35) Shrestha, B.; Coykendall, K.; Li, Y.; Moon, A.; Priyadarshani, P.; Yao, L. Repair of Injured Spinal Cord Using Biomaterial Scaffolds and Stem Cells. *Stem Cell Res. Ther.* **2014**, *5*, 91.
(36) Mohtaram, N. K.; Ko, J.; King, C.; Sun, L.; Muller, N.; Jun, M. B.-G.; Willerth, S. M. Electrospun Biomaterial Scaffolds with Varied Topographies for Neuronal Differentiation of Human-Induced Pluripotent Stem Cells. *J. Biomed. Mater. Res., Part A* **2015**, *103*, 2591−2601.
(37) Ghasemi-Mobarakeh, L.; Prabhakaran, M. P.; Morshed, M.; Nasr-Esfahani, M. H.; Baharvand, H.; Kiani, S.; Al-Deyab, S. S.; Ramakrishna, S. Application of Conductive Polymers, Scaffolds and Electrical Stimulation for Nerve Tissue Engineering. *J. Tissue Eng. Regener. Med.* **2011**, *5*, e17−e35.
(38) Dvir, T.; Timko, B. P.; Kohane, D. S.; Langer, R. Nanotechnological Strategies for Engineering Complex Tissues. *Nat. Nanotechnol.* **2011**, *6*, 13−22.
(39) Khang, D.-Y.; Rogers, J. A.; Lee, H. H. Mechanical Buckling: Mechanics, Metrology, and Stretchable Electronics. *Adv. Funct. Mater.* **2009**, *19*, 1526−1536.
(40) Lee, J. N.; Park, C.; Whitesides, G. M. Solvent Compatibility of Poly(dimethylsiloxane)-Based Microfluidic Devices. *Anal. Chem.* **2003**, *75*, 6544−6554.
(41) Huang, J.; Ichinose, I.; Kunitake, T. Nanocoating of Natural Cellulose Fibers with Conjugated Polymer: Hierarchical Polypyrrole Composite Materials. *Chem. Commun.* **2005**, 1717−1719.
(42) Abidian, M. R.; Kim, D.-H.; Martin, D. C. Conducting-Polymer Nanotubes for Controlled Drug Release. *Adv. Mater.* **2006**, *18*, 405−409.
(43) Carquigny, S.; Segut, O.; Lakard, B.; Lallemand, F.; Fievet, P. Effect of Electrolyte Solvent on the Morphology of Polypyrrole Films: Application to the Use of Polypyrrole in pH Sensors. *Synth. Met.* **2008**, *158*, 453−461.
(44) Ouyang, J.; Li, Y. Effect of Electrolyte Solvent on the Conductivity and Structure of as-Prepared Polypyrrole Films. *Polymer* **1997**, *38*, 1971−1976.
(45) Huang, Z.; Wang, P.-C.; Feng, J.; MacDiarmid, A. G.; Xia, Y.; Whitesides, G. M. Selective Deposition of Films of Polypyrrole, Polyaniline and Nickel on Hydrophobic/hydrophilic Patterned Surfaces and Applications. *Synth. Met.* **1997**, *85*, 1375−1376.
(46) Cairns, D. B.; Khan, M. A.; Perruchot, C.; Riede, A.; Armes, S. P. Synthesis and Characterization of Polypyrrole-Coated Poly(Alkyl Methacrylate) Latex Particles. *Chem. Mater.* **2003**, *15*, 233−239.
(47) Varesano, A.; Rombaldoni, F.; Tonetti, C. Electrically Conductive and Hydrophobic Cotton Fabrics by Polypyrrole-Oleic Acid Coating. *Fibers Polym.* **2013**, *14*, 703−709.
(48) Mawad, D.; Stewart, E.; Officer, D. L.; Romeo, T.; Wagner, P.; Wagner, K.; Wallace, G. G. A Single Component Conducting Polymer Hydrogel as a Scaffold for Tissue Engineering. *Adv. Funct. Mater.* **2012**, *22*, 2692−2699.
(49) Fonner, J. M.; Forciniti, L.; Nguyen, H.; Byrne, J.; Kou, Y.-F.; Syeda-Nawaz, J.; Schmidt, C. E. Biocompatibility Implications of Polypyrrole Synthesis Techniques. *Biomed. Mater.* **2008**, *3*, 034124.
(50) Palacios-Cuesta, M.; Cortajarena, A. L.; García, O.; Rodríguez-Hernández, J. Fabrication of Functional Wrinkled Interfaces from Polymer Blends: Role of the Surface Functionality on the Bacterial Adhesion. *Polymers* **2014**, *6*, 2845−2861.
(51) Yoshimitsu, Z.; Nakajima, A.; Watanabe, T.; Hashimoto, K. Effects of Surface Structure on the Hydrophobicity and Sliding Behavior of Water Droplets. *Langmuir* **2002**, *18*, 5818−5822.
(52) Park, J.; Bauer, S.; Schlegel, K. A.; Neukam, F. W.; von der Mark, K.; Schmuki, P. TiO2 Nanotube Surfaces: 15 nm—An Optimal Length Scale of Surface Topography for Cell Adhesion and Differentiation. *Small* **2009**, *5*, 666−671.
(53) Karuri, N. W.; Liliensiek, S.; Teixeira, A. I.; Abrams, G.; Campbell, S.; Nealey, P. F.; Murphy, C. J. Biological Length Scale Topography Enhances Cell-Substratum Adhesion of Human Corneal Epithelial Cells. *J. Cell Sci.* **2004**, *117*, 3153−3164.
(54) Tay, C. Y.; Irvine, S. A.; Boey, F. Y. C.; Tan, L. P.; Venkatraman, S. Micro-/Nano-Engineered Cellular Responses for Soft Tissue Engineering and Biomedical Applications. *Small* **2011**, *7*, 1361−1378.
(55) den Braber, E. T.; de Ruijter, J. E.; Ginsel, L. A.; von Recum, A. F.; Jansen, J. A. Quantitative Analysis of Fibroblast Morphology on Microgrooved Surfaces with Various Groove and Ridge Dimensions. *Biomaterials* **1996**, *17*, 2037−2044.
(56) Thakar, R. G.; Chown, M. G.; Patel, A.; Peng, L.; Kumar, S.; Desai, T. A. Contractility-Dependent Modulation of Cell Proliferation and Adhesion by Microscale Topographical Cues. *Small* **2008**, *4*, 1416−1424.
(57) Chua, J. S.; Chng, C.-P.; Moe, A. A. K.; Tann, J. Y.; Goh, E. L. K.; Chiam, K.-H.; Yim, E. K. F. Extending Neurites Sense the Depth of

DOI: 10.1021/acsami.5b09355
ACS Appl. Mater. Interfaces 2015, 7, 23454−23463

the Underlying Topography during Neuronal Differentiation and Contact Guidance. *Biomaterials* **2014**, *35*, 7750−7761.
(58) Su, W.-T.; Liao, Y.-F.; Wu, T.-W.; Wang, B.-J.; Shih, Y.-Y. Microgrooved Patterns Enhanced PC12 Cell Growth, Orientation, Neurite Elongation, and Neuritogenesis. *J. Biomed. Mater. Res., Part A* **2013**, *101A*, 185−194.
(59) Foley, J. D.; Grunwald, E. W.; Nealey, P. F.; Murphy, C. J. Cooperative Modulation of Neuritogenesis by PC12 Cells by Topography and Nerve Growth Factor. *Biomaterials* **2005**, *26*, 3639−3644.

DOI: 10.1021/acsami.5b09355
ACS Appl. Mater. Interfaces 2015, 7, 23454−23463